






**Buzdin, Shapiro, and chimera steps in  $\varphi_0$  Josephson junctions**Yu. M. Shukrinov <sup>1,2,3</sup>, E. Kovalenko <sup>4</sup>, J. Tekić <sup>5</sup>, K. Kulikov <sup>1,2</sup> and M. Nashaat <sup>1,6</sup><sup>1</sup>*BLTP, JINR, Dubna, Moscow Region 141980, Russia*<sup>2</sup>*Department of Nanotechnology and New Materials, Dubna State University, Dubna, Russia*<sup>3</sup>*Moscow Institute of Physics and Technology, Dolgoprudny 141700, Russia*<sup>4</sup>*Center for the Development of Digital Technologies, Krasnogorsk, Russia*<sup>5</sup>*“Vinča” Institute of Nuclear Sciences, Laboratory for Theoretical and Condensed Matter Physics - 020, University of Belgrade, PO Box 522, 11001 Belgrade, Serbia*<sup>6</sup>*Department of Physics, Faculty of Science, Cairo University, 12613 Giza, Egypt*

(Received 11 August 2023; revised 12 December 2023; accepted 22 December 2023; published 17 January 2024)

The unique resonance and locking phenomena in the superconductor-ferromagnet-superconductor  $\varphi_0$  Josephson junction under external electromagnetic radiation are demonstrated when not just the electric but also the magnetic component of external radiation is taken into account. Due to the coupling of superconductivity and magnetism in this system, the magnetic moment precession of the ferromagnetic layer caused by the magnetic component of external radiation can lock the Josephson oscillations, which results in the appearance of a particular type of step in the current-voltage characteristics, completely different from the well-known Shapiro steps. We call these steps the Buzdin steps in the case when the system is driven only by the magnetic component and the chimera steps in the case when both magnetic and electric components are present. Unlike the Shapiro steps where the magnetic moment remains constant along the step, here it changes though the system is locked. The spin-orbit coupling substantially contributes to the amplitude, i.e., the size of these steps. Dramatic changes in their amplitudes are also observed at frequencies near the ferromagnetic resonance. Combinations of the Josephson and Kittel ferromagnetic resonances together with different types of locking pronounced in dynamics and current-voltage characteristics make the physics of this system very interesting and open up a series of new applications.

DOI: [10.1103/PhysRevB.109.024511](https://doi.org/10.1103/PhysRevB.109.024511)**I. INTRODUCTION**

The possibility to combine superconductivity and magnetism in hybrid Josephson structures holds promise to increase the technological applications of superconductors and superconducting nanostructures in the recent rapid development of spintronics and superconducting logic devices. Currently, intense activity is focused on identifying combinations of materials and types of superconductor-ferromagnet (SF) structures that enhance device functionality and performance, leading to progress in superconducting spintronics and quantum computation [1,2].

The SF heterostructures exhibit a plethora of interesting physical phenomena, such as spin-triplet superconductivity, superconducting order parameter oscillation, and topological superconductivity [2–4]. Recently the magnon-fluxon interaction and Cherenkov radiation of spin accompanied by a magnon Shapiro step in its current-voltage characteristics were detected in the SF systems [5,6]. Phenomena such as ultrastrong magnon-photon coupling, squeezed vacuum, quantum entanglement, and the Anderson-Higgs mechanism of mass generation were also observed in the SF nanostructures and superconductor-ferromagnet-superconductor (SFS) systems, respectively [7,8]. Due to an inversion symmetry breaking and nonreciprocal behavior, these systems open up a door for the realization of the field-free Josephson diode [9–12].

One particular structure that demonstrates transport properties with disrupting scientific and technological potential is the SFS  $\varphi_0$  Josephson junction (JJ) [13,14]. It belongs to a special class of anomalous JJs with a noncentrosymmetric ferromagnetic layer and broken time-reversal symmetry. These properties result in the occurrence of an additional phase shift  $\varphi_0$  proportional to the magnetic moment [15], and the current-phase relation becomes  $I = I_c \sin(\varphi - \varphi_0)$ , where  $I_c$  is the critical current and  $\varphi$  is the superconducting phase difference. Experimental observations of this anomalous phase shift in different systems [16–18] open up several new opportunities for superconducting spintronics [1]. The presence of *bidirectional* coupling between the magnetic moment of the barrier and the superconducting phase difference allows superconductivity to control magnetism and vice versa, to influence Josephson current via magnetic moment, which could lead to a series of new applications [1,13–15,19–21].

One very distinct phenomenon that appears in this system is the occurrence of the ferromagnetic resonance (FMR), which is innate to the  $\varphi_0$  JJ, and it appears without any external radiation [22,23]. It manifests itself through the dependence of the maximal value of the magnetic component on the bias current, producing a sharp peak while in the current-voltage (*IV*) characteristics it appears as a resonance branch over a voltage interval that characterizes the width of the resonance.

When a  $\varphi_0$  JJ is under external radiation, a very complex behavior appears in the FMR region. As shown in Ref. [22],

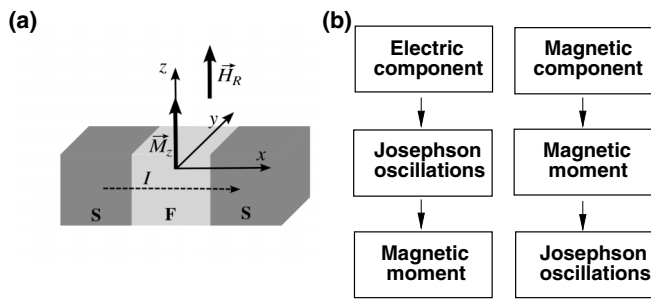


FIG. 1. (a) Geometry of the system. (b) Demonstration of two locking mechanisms in the  $\varphi_0$  Josephson junction under an external electromagnetic field (see the text).

the magnetic precession in the ferromagnetic (F) layer may get locked by external electromagnetic radiation through the locking of the Josephson oscillations. The presence of external radiation also leads to the appearance of additional resonance peaks whose properties depend on the periodic signal and Josephson junction dynamics [24]. These phenomena open up a unique perspective to control and manipulate the magnetic moment and resonance in hybrid SF systems.

In general, in the studies of JJ systems driven by external radiation, the influence of the magnetic component of radiation is usually neglected, and the description of the effect is reduced to adding the term  $I_R \sin(\Omega_R t)$  to the bias current where  $\Omega_R$  is the radiation frequency.

However, contrary to ordinary superconductor-insulator-superconductor (SIS-type) junctions, in the  $\varphi_0$  JJ, as mentioned in Ref. [14], the microwave magnetic field generates an additional magnetic precession with the microwave frequency which might lead to a series of unusual effects. So far these predictions have not been verified and detailed studies of the interaction of electromagnetic radiation with the  $\varphi_0$  junction taking into account the magnetic component have not been carried out. Here we eliminate this shortcoming and include the direct interaction of the magnetic component of the microwave magnetic field with the magnetic moment of the ferromagnetic layer in our study of radiation effects in the  $\varphi_0$  junction. The considered geometry is demonstrated in Fig. 1(a).

In this work, we demonstrate the effects of microwave radiation on the dynamics and the  $IV$  characteristics of the SFS  $\varphi_0$  Josephson junction taking into account both the magnetic and electric components of radiation. This leads to two different mechanisms of locking the Josephson oscillations and the ferromagnetic moment precessions presented in Fig. 1(b): the electric component locks Josephson oscillations which further lock the magnetic moment, while on the other hand, the magnetic component locks the precession of the magnetic moment which then transfers to Josephson oscillations.

These mechanisms of indirect locking are investigated at different parameters of the  $\varphi_0$  junction and microwave field. To get an insight into their mechanisms, we will first consider the two-signal (TS) toy model where the magnetic and electric components come from different sources and can be switched on (off) independently. Then we extend our analysis to real

physical systems of interest for potential experiments or applications.

Within both of these frameworks, in addition to the Shapiro steps caused by the electric component of radiation, we observe a unique step created by the periodic field of the magnetic component. By locking the magnetic moment precession, one can also lock the Josephson oscillations due to their coupling with the ferromagnetic moment. To stress its different origin and properties from the Shapiro step (SS), we call this step the Buzdin step (BS) since this effect of microwave magnetic field in the  $\varphi_0$  Josephson junction was first proposed in Ref. [14]. When both radiation components are taken into account, we observe another type of step, which we name the composite or chimera step due to its creation by two different mechanisms. Below we will call this step simply the CS. We show that CS has specific features reflecting its origin from two different locking mechanisms. While the electric component interacts with the superconducting current, the magnetic component drives the ferromagnetic moment, but in both cases, an important influence comes from the coupling of Josephson oscillations and ferromagnetic moment precession determined by the value of the spin-orbit parameter. We also show that when either Josephson or radiation frequencies approach the ferromagnetic one the interplay of the Josephson and Kittel ferromagnetic resonances appears.

The paper is organized as follows. The model is introduced in Sec. II. The effect of the magnetic component and the properties of Buzdin steps are studied within the two-signal model in Sec. III. The appearance of CS when both components are present is analyzed first within the two-signal toy model and then extended to a real system in Sec. IV. The competition between the Kittel and Josephson ferromagnetic resonance is discussed in Sec. V. Finally, Sec. VI concludes the paper.

## II. MODEL

The dynamics of the system in Fig. 1 is characterized by the coupling between the superconducting phase difference across the junction  $\varphi$  and the magnetization  $\mathbf{M}$  of the ferromagnetic (F) layer. It can be described by the system of equations obtained from the Landau-Lifshitz-Gilbert (LLG) equation, the Josephson relation for the phase difference and voltage, and the equation for the biased current of the resistively and capacitively shunted junction (RCSJ) model [25]. Starting from the pioneering work in Refs. [13,14] as well as our previous studies [26], in this work, we will go further and consider the effect of external radiation taking into account both the magnetic and electric components.

The dynamics of the magnetic moment is determined by the Landau-Lifshitz-Gilbert (LLG) equation [27]:

$$\frac{d\mathbf{M}}{dt} = -\gamma \mathbf{M} \times \mathbf{H}_{\text{eff}} + \frac{\alpha}{M_0} \left( \mathbf{M} \times \frac{d\mathbf{M}}{dt} \right), \quad (1)$$

where  $\gamma$  is the gyromagnetic ratio,  $\alpha$  is the Gilbert damping constant, and  $M_0 = ||\mathbf{M}||$ . The effective magnetic field acting on  $\mathbf{M}$  is given by

$$\mathbf{H}_{\text{eff}} = -\frac{1}{\mathcal{V}} \frac{\delta F}{\delta \mathbf{M}}, \quad (2)$$

where  $F$  is the free energy of the system, and  $\mathcal{V}$  is the volume of the ferromagnet.

The free energy consists of three parts:

$$F = E_S + E_M + E_R, \quad (3)$$

where  $E_S$  is the superconducting energy [14] given as

$$E_S = E_J \left[ 1 - \cos \left( \varphi - r \frac{M_y}{M_0} \right) \right], \quad (4)$$

where  $E_J = \Phi_0 I_c / 2\pi$  is the Josephson energy and  $\Phi_0 = h/2e$  is the flux quantum.

The relative strength of spin-orbit coupling is characterized by the Rashba type parameter  $r$  [14]. The magnetic energy  $E_M$  is reduced to the anisotropy energy:

$$E_M = -\frac{K\mathcal{V}}{2} \left( \frac{M_z}{M_0} \right)^2, \quad (5)$$

where  $K$  is an anisotropy constant. Finally,  $E_R$  represents the energy of the ferromagnet in the magnetic field of the external radiation given as

$$E_R = -(\mathbf{M}, \mathbf{H}_R), \quad (6)$$

where

$$\mathbf{H}_R = (0, 0, H_R \sin(\Omega_R t)); \quad (7)$$

$H_R$  is the amplitude of the radiation magnetic component, and  $\Omega_R$  is the radiation frequency.

Substituting Eqs. (4)–(6) into Eq. (2) we obtain the expression for the effective field:

$$\begin{aligned} \mathbf{H}_{\text{eff}} = & \frac{K}{M_0} Gr \sin \left( \varphi - r \frac{M_y}{M_0} \right) \hat{\mathbf{y}} \\ & + \left( \frac{K}{M_0} \frac{M_z}{M_0} + H_R \sin(\Omega_R t) \right) \hat{\mathbf{z}}, \end{aligned} \quad (8)$$

where  $G = E_J / (K\mathcal{V})$  represents the ratio of the Josephson to magnetic anisotropy energy. The second term inside the sine function represents the phase shift  $\varphi_0 = rM_y/M_0$ . In the geometry presented in Fig. 1, the ferromagnet easy axis and the gradient of the spin-orbit potential are directed along the  $z$  axis. In this case,  $\varphi_0$  is proportional to the  $y$  component of the magnetic moment  $\mathbf{M}$ . The junction is under linearly polarized radiation with frequency,  $\Omega_R$ , and the magnetic component  $\mathbf{H}_R$  is parallel to the  $z$  axis.

We consider the current-biased JJ where the external current  $I$  flows through the system according to the extended RCSJ model [25]. The Josephson relation for the phase difference and voltage is given by  $V = \frac{\hbar}{2e} \frac{d\varphi}{dt}$ . Introducing the dimensionless variables  $m_i = \frac{M_i}{M_0}$  ( $i \equiv x, y, z$ ), the total system of LLG-Josephson equations becomes

$$\begin{aligned} \dot{m}_x = & \frac{1}{\alpha^2 + 1} (\omega_F \{-m_y m_z + Gr m_z \sin(\varphi - r m_y)\} \\ & - \alpha [m_x m_z^2 + Gr m_x m_y \sin(\varphi - r m_y)] \\ & - h_R (\alpha m_x m_z + m_y) \sin(\omega_R t)), \end{aligned}$$

$$\begin{aligned} \dot{m}_y = & \frac{1}{\alpha^2 + 1} (\omega_F \{m_x m_z \\ & - \alpha [m_y m_z^2 - Gr (m_x^2 + m_z^2) \sin(\varphi - r m_y)] \\ & - h_R (\alpha m_y m_z - m_x) \sin(\omega_R t)), \end{aligned}$$

$$\begin{aligned} \dot{m}_z = & \frac{1}{\alpha^2 + 1} (\omega_F \{-Gr m_x \sin(\varphi - r m_y) \\ & - \alpha [Gr m_y m_z \sin(\varphi - r m_y) - m_z (m_x^2 + m_y^2)] \\ & + h_R \alpha (m_x^2 + m_y^2) \sin(\omega_R t)), \\ \dot{V} = & [I + A \sin(\omega_R t) - V(t) + r \dot{m}_y - \sin(\varphi - r m_y)] / \beta_c, \\ \dot{\varphi} = & V(t), \end{aligned} \quad (9)$$

where  $\beta_c = 2eI_c C R^2 / \hbar$  is the McCumber parameter (in our calculations we use  $\beta_c = 25$ ), where  $I_c, C, R$  are the Josephson critical current, the resistance, and the capacitance, respectively. Here, time is normalized in units  $(\omega_c)^{-1}$ , where  $\omega_c = 2eI_c R / \hbar$  is the characteristic frequency of the junction. The ferromagnetic resonance frequency,  $\Omega_F = K\gamma / M_0$ , and the frequency of external radiation  $\Omega_R$  are normalized to  $\omega_c$ , so that  $\omega_F = \frac{\Omega_F}{\omega_c}$  and  $\omega_R = \frac{\Omega_R}{\omega_c}$ , while the amplitude of the magnetic component is then normalized so that  $h_R = \frac{\gamma}{\omega_c} H_R$ . In Eq. (9) the electric component of the external radiation is represented by the ac current source  $A \sin(\omega_R t)$ , where  $A$  is normalized to the critical current  $A = I_R / I_c$ . Finally, the bias current  $I$  and the voltage  $V$  across the junction are normalized to  $I_c$  and  $I_c R$ , respectively. In this normalization the Josephson frequency  $\omega_J = V$ , where  $V$  denotes the time average of the instantaneous voltage  $V(t)$ .

An important point is concerning the gauge invariance of our system of equations (9) for the  $\varphi_0$  Josephson junction. The gauge invariance of these equations without external radiation was discussed in Refs. [28,29]. It was stressed that the term  $r\dot{m}_y$  in the equation for current (9) stems from the time derivative of the anomalous phase  $\varphi_0$  and it was ignored in Refs. [14,30,31], but has to be included to preserve gauge invariance. The detailed derivation of this term can be found in the Supplemental Material of Ref. [28]. In Refs. [32,33] the SFS Josephson junction under the ac magnetic field was investigated and the resistively shunted junction (RSJ) model was extended to include the effect of spin wave excitations by using the gauge-invariant phase difference between superconducting leads. Generally, the external magnetic field produces additional phase shift in terms of the vector potential  $A$  which is given by  $-2\pi\Phi_0 \int \mathbf{A} \cdot d\mathbf{l}$  [34]. According to the recently proposed recipe in Ref. [35] on how to properly account for driving by the time-dependent electromagnetic field, we would expect that in our system, an additional shift should appear in the Josephson energy and consequently the Josephson supercurrent. However, this is not the case. Due to the chosen geometry (magnetic field in the  $z$  direction), in our system, only the current-phase relation contains the additional phase  $r m_y$ , and the additional term  $r\dot{m}_y$  in the equation for current appears due to the gauge invariance.

This system of equations (9) is solved numerically using the fourth-order Runge-Kutta method, which yields  $m_i(t)$ ,  $V(t)$ , and  $\varphi(t)$  as a function of the external bias current  $I$ . After using the averaging procedure Refs. [36,37] we can find the  $IV$  characteristic at the fixed system parameters. Dynamics is analyzed in different cases when only the magnetic component or both the electric and magnetic ones affect the system.

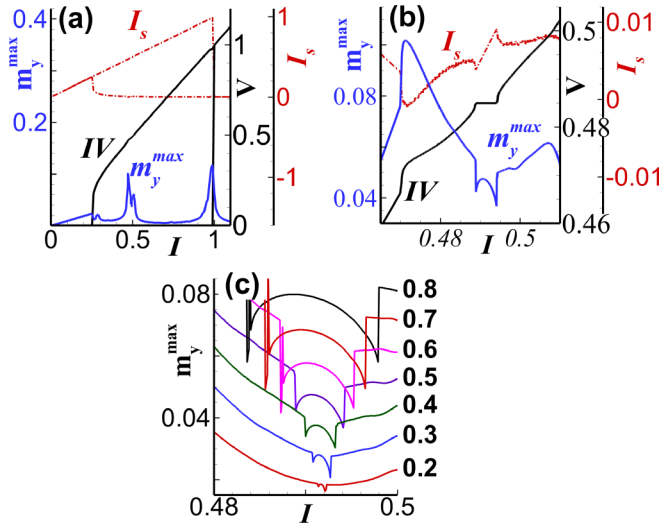


FIG. 2. The average voltage  $V$ , the maximum value of the  $m_y$  magnetic component  $m_y^{\max}$ , and the superconducting current  $I_s$  as a function of decreasing biased current  $I$  for  $A = 0$ ,  $h_R = 1$ ,  $r = 0.5$ ,  $G = 0.01$ ,  $\alpha = 0.01$ ,  $\omega_R = 0.485$ , and  $\omega_F = 0.5$ . (b) Magnified view of (a) showing the Buzdin step. (c)  $m_y^{\max}$  at different values of  $r$ .

### III. THE EFFECT OF MAGNETIC COMPONENT: BUZDIN STEPS

First, let us examine the effects of the magnetic component of external radiation (MCR) on the magnetization dynamics and the  $IV$  characteristics in the ferromagnetic resonance region when the resonance frequency is close to the Josephson one, i.e.,  $\omega_F \approx \omega_J$ . Unlike the electric component, the magnetic one can interact directly with the magnetic moment of the ferromagnetic barrier, which further leads to the appearance of the Buzdin step in the  $IV$  characteristics. To get an insight into the origin of BS, we start with the TS model and switch off the term  $A \sin(\omega_R t)$ , which describes the influence of the electric component of radiation, and investigate the effect of  $h_R$  only; i.e., we concentrate on the features produced by MCR.

The average voltage  $V$ , the maximum value of the magnetic moment  $m_y^{\max}$ , and the superconducting current  $I_s$  as functions of decreasing biased current  $I$  are presented in Fig. 2(a). It shows the ferromagnetic resonance and its manifestation in these characteristics. The magnified view of Fig. 2(a) in the FMR region with the Buzdin step is presented in Fig. 2(b). Its appearance is a result of the locking of Josephson oscillations by the magnetic component of external radiation. Namely, the MCR creates the periodic precession of the magnetic moment, which then, through coupling with Josephson oscillations, also locks the Josephson oscillations. So, due to their bidirectional coupling, both the Josephson oscillations and the magnetic precession are locked with MCR. The specific manifestation of this locking is also seen in the  $I_s(I)$  in the current interval corresponding to the Buzdin step, and in  $m_y^{\max}(I)$ , where the magnified view reveals a ‘‘bubble-like’’ feature due to changing of  $m_y^{\max}$  along the step (we will further use the term ‘‘bubble’’ as a name for this particular change of magnetization along the step). So, we observe the locking of

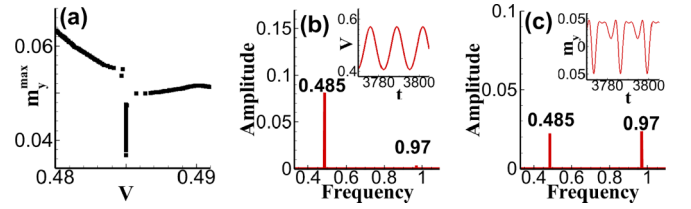


FIG. 3. (a)  $m_y^{\max}$  as a function of  $V$ . (b) and (c) The time dependence of  $V$  and  $m_y$ , and the corresponding FFT analysis in the center of the bubble, respectively. Other parameters are as in Fig. 2.

the magnetic moment precession with a changed amplitude but fixed frequency, which is stressed below in Fig. 3(a).

An interesting question is related to the variation of the parameters characterizing the interaction of Josephson oscillations with the magnetic moment, in particular, the spin-orbit coupling  $r$ . This parameter plays a key role in the appearance of the Buzdin step since it is the coupling between the magnetic moment and Josephson oscillation through which the locking of the magnetic moment transfers to the superconducting subsystem. Of course, if  $r = 0$  there is no coupling, and the Buzdin step does not exist. In Fig. 2(c), the variation  $m_y^{\max}(I)$  at different parameters of spin-orbit coupling is presented, where the focus was on the changes of the bubble structure under  $r$ . We know from Fig. 2(b) that the width of the bubble exactly corresponds to the width of the Buzdin step, which increases with an increase in the spin-orbit coupling.

The proof of the locking by MCR can be seen in Fig. 3(a), where the voltage dependence of  $m_y^{\max}$  is presented. As we can see, there is a sharp minimum at the same value of voltage (i.e., frequency) corresponding to the Buzdin step. The time dependence of  $V$  and  $m_y$  and the corresponding fast Fourier transform (FFT) analysis in Figs. 3(b) and 3(c), respectively, further confirm the locking by MCR.

### IV. THE EFFECT OF MAGNETIC AND ELECTRIC COMPONENTS: CHIMERA STEPS

Let us now discuss the effects of both electric and magnetic components of electromagnetic radiation on the  $IV$  characteristics and magnetization dynamics of the  $\varphi_0$  JJ. In this case, the irradiation of the  $\varphi_0$  JJ leads to the realization of two different mechanisms of locking. In one of them, the electric component of radiation locks the Josephson oscillations, and this, due to their coupling with the magnetic moment, locks the precession of the magnetic moment of the ferromagnetic barrier [22]. In the second mechanism, the periodic field of the magnetic component through the interaction with the magnetic moment locks the Josephson oscillations leading to the Buzdin steps in the  $IV$  characteristics. The combined effect of both components results in the appearance of a unique step different from BS and SS. As mentioned above, since it comes from two different mechanisms of locking, we call this step the composite or chimera step.

To get a better insight, we first examine the effect of electromagnetic radiation in the framework of the TS model. Figure 4(a) demonstrates the effect of both the electric and magnetic components of radiation at  $r = 0.2$ ,  $h_R = 1$ , and  $A = 0.01$ . It shows the  $IV$  characteristics and  $m_y^{\max}(I)$



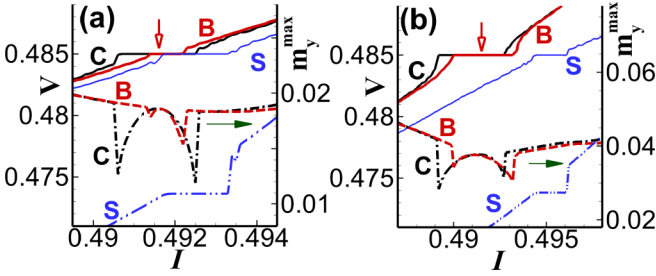


FIG. 4. The effects of both radiation components. (a) Parts of  $IV$  characteristics with the Buzdin (label B), Shapiro (label S), and composite (label C) steps at  $r = 0.2$ . (b) The same at  $r = 0.4$ . Other parameters are as in Fig. 2.

dependence for three cases: (i) in the presence of two components; (ii) the electric component only; and (iii) the magnetic component only. We stress that the CS is not a trivial sum of BS and SS. In particular, we see in its left part that it does not coincide with SS and BS under separate actions. The corresponding  $m_y^{\max}(I)$  dependence shows the bubble structure, which indicates that in this case, we observe also a locking with variable amplitude of the magnetization precession. Surprisingly the bubble structure continues along the whole CS because, in the second and third cases, we have seen the bubble structure for the BS, and the locking step for SS, where  $m_y^{\max}$  stays constant along the step. In this figure, the scale of the  $m_y^{\max}(I)$  dependence for the first and third cases is the same, while in the second case, we have made an arbitrary shift to show clearly the manifestation of SS. An important fact here is that the maximal amplitude of the magnetization precession is the same in BS and CS; i.e., CS conserves this characteristic of the magnetic component effect. We stress also that the size of the Shapiro step does not change with the spin-orbit parameter.

As we see, BS is smaller than SS at these model parameters. We show in Fig. 2(c) that the value of BS is growing with  $r$ . So by variation of the  $\varphi_0$  junction and external radiation parameters, we expect the case when BS is larger than SS. This case is shown in Fig. 4(b) at  $r = 0.4$ . Additionally, SS calculated at  $h_R = 0$  is in the current interval, which is out of the corresponding interval for the CS. Like in Fig. 4(a), we have shifted arbitrarily the  $m_y^{\max}(I)$  dependence for clarity.

In Fig. 5(a), the  $IV$  characteristics and  $m_y^{\max}$  are plotted when both radiation components are switched on for three cases of different amplitudes of electric components. We observe a fast increase in the CS width with the amplitude of the electric component.

So far we have only considered the region near FMR  $\omega_F = 0.5$  at  $\omega_R = 0.485$ , which leads to the question of how the behavior changes when the frequency of external radiation is equal to the ferromagnetic resonant one. In Fig. 5(b) the  $IV$  characteristics and  $m_y^{\max}$  are presented for the magnetic component only ( $A = 0$ ) at  $\omega_R = \omega_F = 0.5$ . The Buzdin step in the  $IV$  characteristics and its locking signature (the bubble structure) in the  $m_y^{\max}(I)$  dependence can be seen clearly.

Up to this point, we considered the TS toy model where each component of radiation can be switched on (off) independently. Let us now discuss the real situation of one electromagnetic signal when both components of the electro-

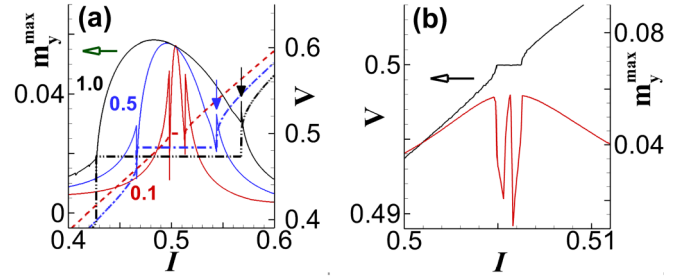


FIG. 5. (a) The  $IV$  characteristics and  $m_y^{\max}$  for three cases of different amplitudes of the electric components indicated by numbers. Other parameters are  $G = 0.01$ ,  $r = 0.2$ , and  $h_R = 1$ . (b) The  $IV$  characteristics and  $m_y^{\max}$  as a function of  $I$  in the case of the magnetic components only for  $\omega_R = \omega_F = 0.5$ .

magnetic wave are taken into account and their amplitudes correspond to the real relation between them. In particular, the oscillations of the components are synchronized and the density of energy of the electromagnetic wave is expressed through them as  $w = \epsilon E_R^2 = H_R^2/\mu$ , where  $\epsilon$  is the permittivity (F/m) of the material,  $E_R$  is the electric field strength (V/m),  $\mu$  is the permeability (H/m), and  $H_R$  the magnetic field strength (T).

In materials such as permalloy doped with Pt [38] or the ferromagnets MnSi and FeGe, the value of  $r$  can vary in the range 0.1–1 [39]. In the material with weak magnetic anisotropy  $K \sim 4 \times 10^{-5} \text{ KA}^{-3}$  [40], the value of the product  $Gr$  can be in the range 0.01–100 [14]. There is a way to enlarge the value of spin-orbit coupling if we put the  $\varphi_0$  JJ on the surface of the 3D topological insulator. In this case, the SOC coefficient  $r$  has been estimated in Refs. [41,42] to be up to 10.

If we assume critical current density  $J_c = 10^5 \text{ A/cm}^2$ , JJ area  $(0.1 \times 0.1) \mu\text{m}^2$ , and resistance  $R = 1 \Omega$ , then the characteristic frequency is  $\omega_c = 30 \text{ GHz}$ . With microwave power  $P \approx 10^{-10} \text{ W}$ , using the approximated relation  $P = (AI_c)^2$ , we get the value of  $A = 1$ . As was mentioned in Refs. [37,43,44], the constant of proportionality between  $P$  and  $A$  depends on many unknown parameters like temperature dependence and nonlinearities of the subgap resistance, the junction capacitance, the thermal conductance, and the junction geometry. By using the relation between  $P$  and  $A$ , one can find the relation between  $h_R$  and  $A$ :

$$h_R = \frac{\gamma I_c A}{v^{3/2} \omega_c} \sqrt{\frac{2R}{S\epsilon}}, \quad (10)$$

where  $v = 1/\sqrt{\mu\epsilon}$ , and  $S$  is the area of the JJ. Within the given estimations for the model parameters and considering the magnetic permeability within  $10^2 \sim 10^5$ , we might have the values  $A = 1$  and  $h_R$  in the interval (0.002–0.298) for power  $P = 10^{-10} \text{ W}$ . The power  $P = 10^{-8} \text{ W}$  leads to the values  $A = 10$  and  $h_R$  in the interval (0.017–2.982).

Figure 6(a) presents the  $IV$  characteristics and  $m_y^{\max}$  dependence on the bias current for  $A = 3$  and the corresponding value  $h_R \approx 0.9$  at spin-orbit parameter  $r = 0.2$ . For comparison, we plot here the results for the Buzdin and Shapiro steps in a two-signal model as well. We see that the CS and SS have practically the same width, while the BS is very small. But,

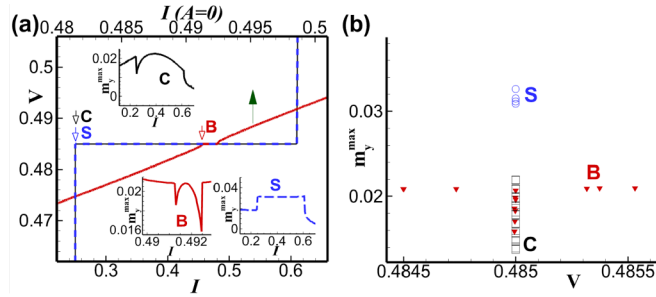


FIG. 6. (a) Demonstration of the Shapiro (label S), Buzdin (label B), and chimera (label C) on the  $IV$  characteristics, and the manifestation of the electric and (or) magnetic components on  $m_y^{\max}$  at  $A = 3$ ,  $h_R = 0.9$ ,  $G = 0.01$ ,  $r = 0.2$ , and  $\omega_R = 0.485$ . (b)  $m_y^{\max}$  as a function of voltage at the same parameters.

the important point here is the fact that there is a pronounced effect of the magnetic component on the  $m_y^{\max}(I)$  dependence. It exhibits the bubble structure along the chimera step as it was observed along the Buzdin step in the TS model.

Figure 6(b) proves that we observe locking phenomena at  $V = 0.485$  when  $\omega_R = \omega_J$ . The locking of magnetic moment precession to the Josephson oscillations and microwave magnetic field happens simultaneously. As in the TS model, the locking of the magnetic moment precession corresponding to the chimera step happens with a changing amplitude of precession. The interval of amplitude changing within the chimera step is practically the same as in the case of the Buzdin step, but very small for the Shapiro one. As it was predicted in Ref. [14], the obtained results demonstrate that the microwave magnetic field may generate an additional magnetic precession with radiation frequency and that two different precession mechanisms related to the Josephson current and microwave radiation are realized.

According to Ref. [14], an increase in the spin-orbit coupling parameter should make the effect of the magnetic component stronger. To have a more pronounced difference between Shapiro and chimera steps, we need to take the  $A$  value corresponding to the smallest Shapiro step and to take the  $h_R$  value which gives the largest Buzdin step. These values can be taken from the Bessel-like amplitude dependence of the step width. Our estimations using the fact that the width of SS is proportional to  $2I_c|J_1(A/\omega)|$  [37], where  $J_1(x)$  is the Bessel function of the first kind,  $\omega = \omega_R[1 + (\beta_c\omega_R)^2]^{1/2}$ , so for  $\beta_c = 25$  and  $\omega_R = 0.47$ , we have the first minimum around  $A \approx 20$  and the second one around  $A = 38.9$  corresponding to  $h_R = 1.64$ .

In Fig. 7(a), the  $IV$  characteristics and  $m_y^{\max}$  dependence on the bias current at  $r = 1$  for the estimated values of parameters  $A = 38.9$  and  $h_R \approx 1.64$  are presented. We see that in this case, the width of the CS is larger than that of the SS. Contrary to the results presented in Fig. 6(a), some variations of  $m_y^{\max}$  along the Shapiro step appear. We consider it to be the result of the coupling between the Josephson oscillations and the magnetic moment precession. So, we come to an important feature concerning the role of the spin-orbit coupling on magnetic dynamics along the Shapiro step.

The locking of the magnetic moment precession to the Josephson oscillations and microwave magnetic field

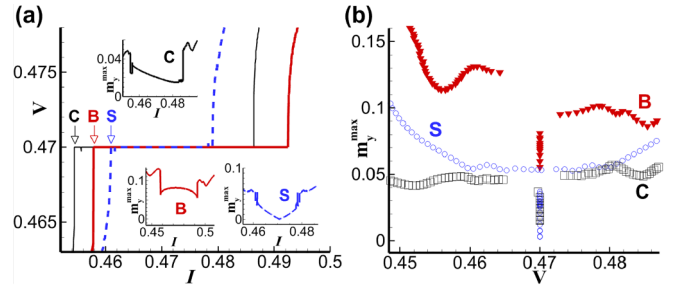


FIG. 7. (a) Demonstration of the Shapiro (label S), Buzdin (label B), and chimera (label C) steps on the  $IV$  characteristics and the variation of  $m_y^{\max}$  along the steps at  $A = 38.9$ ,  $h_R = 1.64$ ,  $G = 0.01$ ,  $r = 1$ , and  $\omega_R = 0.47$ . (b)  $m_y^{\max}$  as a function of voltage at the same parameters.

simultaneously at  $V = 0.47$  is also proven in Fig. 7(b). We stress as well that the results presented here and in Fig. 6(b) qualitatively agree with the results of the two-signal model, shown in Sec. III and Fig. 4 of this section. For that reason, these results could motivate the realization of the two-signal model and the observation of Buzdin steps experimentally. In this case, we would have a decoupling between  $A$  and  $h_R$  [45] and additional possibilities for experimental investigations of SFS  $\varphi_0$  Josephson junctions. So, depending on the junction area, Josephson characteristic frequency, parameters of ferromagnetic material, and radiation power, we expect to see different effects of the magnetic component in the  $IV$  characteristics of the chimera step and the magnetization dynamics of the ferromagnetic layer.

## V. KITTEL VERSUS JOSEPHSON FERROMAGNETIC RESONANCE

Locking is not the only effect that the microwave magnetic field may have on the system. Namely, its direct influence on the magnetic moment of the ferromagnetic layer leads to the Kittel ferromagnetic resonance [46]. Recently, a dramatic increase of the Kittel FMR frequency due to the coupling of magnetization dynamics and superconducting imaginary conductance at the SF interfaces was predicted [8] and confirmed experimentally [47].

On the other hand, the direct coupling of the magnetic moment and Josephson oscillations realized in the  $\varphi_0$  JJ leads to Josephson ferromagnetic resonance with unique features such as the appearance of Shapiro-like steps in the  $IV$  characteristics [32,33,48], different stable magnetic trajectories, and the Duffing oscillator [14,23,31].

Here we show the manifestations of these, the Kittel and Josephson FMRs in the  $\varphi_0$  JJ under external electromagnetic radiation. The effective field in the normalized units has the following components:  $h_x = 0$ ,  $h_y = Gr \sin(\varphi - rm_y) + h_R \sin(\omega_R t)$ , and  $h_z = m_z$ . The results of calculations are presented in Fig. 8, which shows the competition between the Kittel and Josephson FMRs at different model parameters. At rather small values of the magnetic component amplitude  $h_R$  and the Gilbert damping  $\alpha$ , the Kittel resonance (KR) and Josephson resonance (JR) are centered at  $\omega_R = \omega_F$  at different  $\omega_J$ , and at  $\omega_J = \omega_F$  at different  $\omega_R$ , respectively [see

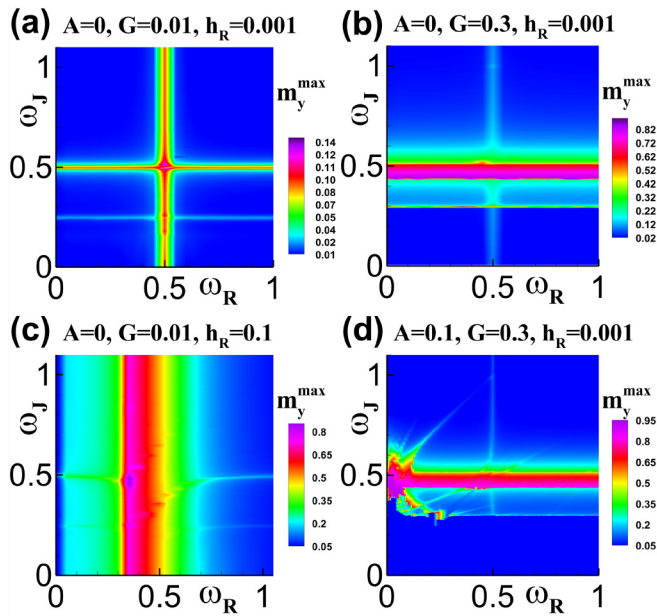


FIG. 8. The competition of the Kittel and Josephson FMRs at  $r = 0.2$  and different model parameters: (a) with varying  $\omega_J$  and  $\omega_F$ , respectively; (b) domination of Josephson resonance at  $G = 0.3$ ; (c) domination of Kittel resonance at  $h_R = 0.1$ ; (d) the effect of both electromagnetic wave components.

Fig. 8(a)]. We can also see a manifestation of a subharmonic peak at  $\omega_J = \omega_F/2$ , which appears as the horizontal line. As discussed before, close to the resonance condition  $\omega_J = \omega_F$ , we observe the locking of the Josephson oscillations and magnetic moment precession. With an increase in the ratio of Josephson to magnetic energy  $G$ , the JR region dominates and the KR region becomes faint [see Fig. 8(b)]. The situation is reversed with increasing  $h_R$  when the KR dominates.

In addition to the shift in the resonance frequency due to magnetic anisotropy [46], the KR region broadens and becomes nonsymmetric around the resonance frequency as shown in Fig. 8(c). The situation changes dramatically when we take into account both the electric and magnetic components of the microwave field. In this case, a crossed resonance region appears, which corresponds to subharmonics and resonances with a combination of  $\omega_F$  and  $\omega_R$  frequencies. In addition to this, by comparing Fig. 8(b) and Fig. 8(d), the effect of  $A$  is manifested in the JR linewidth. So by changing the frequency and amplitude of the external electromagnetic radiation, one can tune and manipulate the Kittel and Josephson resonances in the hybrid Josephson junctions.

Experimentally, the FMR in SFS structures has attracted much attention recently [47,49–51]. The Kittel regime [52] can be used to realize a magnetic logic gate through the superconducting phase transition. A gate-controlled time-dependent spin-orbit coupling is proposed and demonstrated

in Ref. [53]. A dramatic change in current-phase relations and Josephson energy can be seen in this case, even without the bias current. We expect that with these results and the data from the experimental work in Ref. [18], one can tune the chimera step by tuning SOC in hybrid SFS systems.

## VI. CONCLUSION

The magnetic component of radiation brings a series of unique effects in the dynamics of the  $\varphi_0$  Josephson junction. Unlike the electric component which leads to the Shapiro steps, the magnetic one can interact directly with the magnetic moment of the ferromagnetic layer and due to its coupling with the superconducting phase can lock the Josephson oscillations creating the Buzdin steps in the  $IV$  characteristics. While for Shapiro steps magnetization remains constant, for Buzdin steps the locking of the magnetization precession is characterized by its changing amplitude, i.e., the appearance of bubble structure along the step. The spin-orbit coupling substantially contributes to the amplitude of the Buzdin steps, which exhibits a dramatic increase at frequencies near the ferromagnetic resonance. If both (magnetic and electric) components drive the system, the presence of two locking mechanisms leads to the novel type of steps, the chimera steps.

When the analysis is performed in a real system where both components are related and come from the same electromagnetic signal the obtained results exhibit very good agreement with those obtained in the two-signal toy model. Thus we hope that by working within one specific model as well as in a real system, these results could not only justify the application and validity of the two-signal toy model but also represent a theoretical guideline for future experimental studies.

The Buzdin, Shapiro, and chimera steps have different properties (magnetization dynamics along the step, amplitude dependence, etc.), and we consider them to be interesting both from theoretical and experimental points of view. Also, the specific combinations of the Josephson and Kittel ferromagnetic resonances in the  $\varphi_0$  Josephson junctions and the different types of locking near these resonances could open up a series of new applications.

## ACKNOWLEDGMENTS

We thank A. Buzdin, I. Rahmonov, and T. Belgibaev for fruitful discussion. Numerical simulations were funded by the Russian Science Foundation Project No. 22-71-10022. J. T. would like to acknowledge the financial support by the Ministry of Education, Science, and Technological Development of the Republic of Serbia, Grant No. 451-03-47/2023-01/200017 (“Vinča” Institute of Nuclear Sciences, University of Belgrade). Special thanks to BLTP, HybriLIT heterogeneous computing platform (LIT, JINR Russia), and Bibliotheca Alexandrina (Egypt) for the HPC servers.

[1] J. Linder and J. W. A. Robinson, Superconducting spintronics, *Nat. Phys.* **11**, 307 (2015).

[2] R. Cai, I. Žutić, and W. Han, Superconductor/ferromagnet heterostructures: A platform for superconducting spintronics and

quantum computation, *Adv. Quantum Technol.* **6**, 2200080 (2023).

[3] A. Fornieri, A. M. Whiticar, F. Setiawan, E. Portolés, A. C. C. Drachmann, A. Keselman, S. Gronin, C. Thomas, T. Wang, R.



- Kallaher *et al.*, Evidence of topological superconductivity in planar Josephson junctions, *Nature (London)* **569**, 89 (2019).
- [4] H. Ren, F. Pientka, S. Hart, A. T. Pierce, M. Kosowsky, L. Lunczer, R. Schlereth, B. Scharf, E. M. Hankiewicz, L. W. Molenkamp *et al.*, Topological superconductivity in a phase-controlled Josephson junction, *Nature (London)* **569**, 93 (2019).
- [5] O. V. Dobrovolskiy, R. Sachser, T. Brächer, T. Böttcher, V. V. Kruglyak, R. V. Vovk, V. A. Shklovskij, M. Huth, B. Hillebrands, and A. V. Chumak, Magnon-fluxon interaction in a ferromagnet/superconductor heterostructure, *Nat. Phys.* **15**, 477 (2019).
- [6] O. V. Dobrovolskiy, Q. Wang, D. Yu. Vodolazov, B. Budinska, R. Sachser, A. V. Chumak, M. Huth, and A. I. Buzdin, Cherenkov radiation of spin waves by ultrafast moving magnetic flux quanta, [arXiv:2103.10156](https://arxiv.org/abs/2103.10156).
- [7] M. Silaev, Ultrastrong magnon-photon coupling, squeezed vacuum, and entanglement in superconductor/ferromagnet nanostructures, *Phys. Rev. B* **107**, L180503 (2023).
- [8] M. Silaev, Anderson-Higgs mass of magnons in superconductor-ferromagnet-superconductor systems, *Phys. Rev. Appl.* **18**, L061004 (2022).
- [9] H. Wu, Y. Wang, Y. Xu, P. K. Sivakumar, C. Pasco, U. Filippozzi, S. S. P. Parkin, Y. J. Zeng, T. McQueen, and M. N. Ali, The field-free Josephson diode in a van der Waals heterostructure, *Nature (London)* **604**, 653 (2022).
- [10] C. Baumgartner, L. Fuchs, A. Costa, S. Reinhardt, S. Gronin, G. C. Gardner, T. Lindemann, M. J. Manfra, P. E. Faria Junior, D. Kochan *et al.*, Supercurrent rectification and magnetochiral effects in symmetric Josephson junctions, *Nat. Nanotechnol.* **17**, 39 (2022).
- [11] T. Golod and V. M. Krasnov, Demonstration of a superconducting diode-with-memory, operational at zero magnetic field with switchable nonreciprocity, *Nat. Commun.* **13**, 3658 (2022).
- [12] A. Maiani, K. Flensberg, M. Leijnse, C. Schrade, S. Vaitiekėnas, and R. S. Souto, Nonsinusoidal current-phase relations in semiconductor–superconductor–ferromagnetic insulator devices, *Phys. Rev. B* **107**, 245415 (2023).
- [13] A. I. Buzdin, Direct coupling between magnetism and superconducting current in the Josephson  $\varphi_0$  junction, *Phys. Rev. Lett.* **101**, 107005 (2008).
- [14] F. Konschelle and A. I. Buzdin, Magnetic moment manipulation by a Josephson current, *Phys. Rev. Lett.* **102**, 017001 (2009).
- [15] Yu. M. Shukrinov, Anomalous Josephson effect, *Phys. Usp.* **65**, 317 (2022).
- [16] D. B. Szombati, S. Nadj-Perge, D. Car, S. R. Plissard, E. P. A. M. Bakkers, and L. P. Kouwenhoven, Josephson  $\varphi_0$ -junction in nanowire quantum dots, *Nat. Phys.* **12**, 568 (2016).
- [17] A. Assouline, C. Feuillet-Palma, N. Bergeal, T. Zhang, A. Mottaghizadeh, A. Zimmers, E. Lhuillier, M. Eddrie, P. Atkinson, M. Aprili *et al.*, Spin-orbit induced phase-shift in  $\text{Bi}_2\text{Se}_3$  Josephson junctions, *Nat. Commun.* **10**, 126 (2019).
- [18] W. Mayer, M. C. Dartiailh, J. Yuan, K. S. Wickramasinghe, E. Rossi, and J. Shabani, Gate controlled anomalous phase shift in Al/InAs Josephson junctions, *Nat. Commun.* **11**, 212 (2020).
- [19] A. S. Melnikov, S. V. Mironov, A. V. Samokhvalov, A. I. Buzdin *et al.*, Superconducting spintronics: Current state and prospects, *Usp. Fiz. Nauk* **192**, 1339 (2022).
- [20] A. I. Buzdin, Proximity effects in superconductor-ferromagnet heterostructures, *Rev. Mod. Phys.* **77**, 935 (2005).
- [21] I. V. Bobkova, A. M. Bobkov, and M. A. Silaev, Magnetoelectric effects in Josephson junctions, *J. Phys.: Condens. Matter* **34**, 353001 (2022).
- [22] S. A. Abdelmoneim, Yu. M. Shukrinov, K. V. Kulikov, H. ElSamman, and M. Nashaat, Locking of magnetization and Josephson oscillations at ferromagnetic resonance in a  $\varphi_0$  junction under external radiation, *Phys. Rev. B* **106**, 014505 (2022).
- [23] Yu. M. Shukrinov, I. R. Rahmonov, A. Janalizadeh, and M. R. Kolahchi, Anomalous Gilbert damping and duffing features of the superconductor-ferromagnet-superconductor  $\varphi_0$  Josephson junction, *Phys. Rev. B* **104**, 224511 (2021).
- [24] K. V. Kulikov, D. V. Anghel, M. Nashaat, M. Dolineanu, M. Sameh, and Yu. M. Shukrinov, Resonance phenomena in a nanomagnet coupled to a Josephson junction under external periodic drive, [arXiv:2307.10989](https://arxiv.org/abs/2307.10989).
- [25] M. Tinkham, *Introduction to Superconductivity*, 2nd ed. (McGraw-Hill Inc, Singapore, 1996).
- [26] A. E. Botha, Yu. M. Shukrinov, J. Tekić, and M. R. Kolahchi, Chaotic dynamics from coupled magnetic monodomain and Josephson current, *Phys. Rev. E* **107**, 024205 (2023).
- [27] E. M. Lifshitz and L. P. Pitaevskii, *Course of Theoretical Physics: Theory of the Condensed State* (Butterworth-Heinemann, Oxford, 1991).
- [28] D. S. Rabinovich, I. V. Bobkova, A. M. Bobkov, and M. A. Silaev, Resistive state of superconductor-ferromagnet-superconductor Josephson junctions in the presence of moving domain walls, *Phys. Rev. Lett.* **123**, 207001 (2019).
- [29] C. Guarcello and F. S. Bergeret, Cryogenic memory element based on an anomalous Josephson junction, *Phys. Rev. Appl.* **13**, 034012 (2020).
- [30] Yu. M. Shukrinov, I. R. Rahmonov, K. Sengupta, and A. Buzdin, Magnetization reversal by superconducting current in  $\varphi$  Josephson junctions, *Appl. Phys. Lett.* **110**, 182407 (2017).
- [31] Yu. M. Shukrinov, I. R. Rahmonov, and K. Sengupta, Ferromagnetic resonance and magnetic precessions in  $\varphi_0$  junctions, *Phys. Rev. B* **99**, 224513 (2019).
- [32] M. Nashaat, A. E. Botha, and Yu. M. Shukrinov, Devil's staircases in the IV characteristics of superconductor/ferromagnet/superconductor Josephson junctions, *Phys. Rev. B* **97**, 224514 (2018).
- [33] S. E. Barnes, M. Aprili, I. Petković, and S. Maekawa, Ferromagnetic resonance with a magnetic Josephson junction, *Supercond. Sci. Technol.* **24**, 024020 (2011).
- [34] L. Cai and E. M. Chudnovsky, Interaction of a nanomagnet with a weak superconducting link, *Phys. Rev. B* **82**, 104429 (2010).
- [35] R.-P. Riwar and D. P. DiVincenzo, Circuit quantization with time-dependent magnetic fields for realistic geometries, *npj Quantum Inf.* **8**, 36 (2022).
- [36] Yu. M. Shukrinov, F. Mahfouzi, and N. F. Pedersen, Investigation of the breakpoint region in stacks with a finite number of intrinsic Josephson junctions, *Phys. Rev. B* **75**, 104508 (2007).
- [37] W. Buckel and R. Kleiner, *Superconductivity: Fundamentals and Applications* (John Wiley & Sons, 2008).
- [38] A. Hrabec, F. J. T. Gonçalves, C. S. Spencer, E. Arenholz, A. T. N'Diaye, R. L. Stamps, and C. H. Marrows, Spin-orbit interaction enhancement in permalloy thin films by Pt doping, *Phys. Rev. B* **93**, 014432 (2016).



- [39] R. W. Greening, D. A. Smith, Y. Lim, Z. Jiang, J. Barber, S. Dail, J. J. Heremans, and S. Emori, Current-induced spin-orbit field in permalloy interfaced with ultrathin Ti and Cu, *Appl. Phys. Lett.* **116**, 052402 (2020).
- [40] A. Yu. Rusanov, M. Hesselberth, J. Aarts, and A. I. Buzdin, Enhancement of the superconducting transition temperature in Nb/permalloy bilayers by controlling the domain state of the ferromagnet, *Phys. Rev. Lett.* **93**, 057002 (2004).
- [41] I. V. Bobkova, A. M. Bobkov, I. R. Rahmonov, A. Mazanik, K. Sengupta, and Yu. M. Shukrinov, Magnetization reversal in superconductor/insulating ferromagnet/superconductor Josephson junctions on a three-dimensional topological insulator, *Phys. Rev. B* **102**, 134505 (2020).
- [42] D. S. Rabinovich, I. V. Bobkova, and A. M. Bobkov, Electrical response of superconductor/ferromagnet/topological-insulator/superconductor junctions to magnetic texture dynamics, *Phys. Rev. B* **101**, 054517 (2020).
- [43] S. Chen, W. Tian, Z. Xu, P. Zhang, H. Du, Z. Wei, D. Li, Y. Lv, H. Sun, Y.-L. Wang *et al.*, Microwave response of NbSe<sub>2</sub> van der Waals Josephson junctions, *Phys. Rev. B* **104**, 214512 (2021).
- [44] Y. Yao, R. Cai, S.-H. Yang, W. Xing, Y. Ma, M. Mori, Y. Ji, S. Maekawa, X.-C. Xie, and W. Han, Half-integer Shapiro steps in strong ferromagnetic Josephson junctions, *Phys. Rev. B* **104**, 104414 (2021).
- [45] S. Mai, E. Kandelaki, A. F. Volkov, and K. B. Efetov, Interaction of Josephson and magnetic oscillations in Josephson tunnel junctions with a ferromagnetic layer, *Phys. Rev. B* **84**, 144519 (2011).
- [46] Charles Kittel, *Introduction to Solid State Physics* (John Wiley & Sons, 2005).
- [47] I. A. Golovchanskiy, N. N. Abramov, V. S. Stolyarov, V. I. Chichkov, M. Silaev, I. V. Shchetinin, A. A. Golubov, V. V. Ryazanov, A. V. Ustinov, and M. Yu. Kupriyanov, Magnetization dynamics in proximity-coupled superconductor-ferromagnet-superconductor multilayers, *Phys. Rev. Appl.* **14**, 024086 (2020).
- [48] S. Hikino, M. Mori, S. Takahashi, and S. Maekawa, Microwave-induced supercurrent in a ferromagnetic Josephson junction, *Supercond. Sci. Technol.* **24**, 024008 (2011).
- [49] I. A. Golovchanskiy, N. N. Abramov, O. V. Emelyanova, I. V. Shchetinin, V. V. Ryazanov, A. A. Golubov, and V. S. Stolyarov, Magnetization dynamics in proximity-coupled superconductor-ferromagnet-superconductor multilayers. II. Thickness dependence of the superconducting torque, *Phys. Rev. Appl.* **19**, 034025 (2023).
- [50] L.-L. Li, Y.-L. Zhao, X.-X. Zhang, and Y. Y. Sun, Possible evidence for spin-transfer torque induced by spin-triplet supercurrents, *Chin. Phys. Lett.* **35**, 077401 (2018).
- [51] K.-R. Jeon, C. Ciccarelli, H. Kurebayashi, L. F. Cohen, X. Montiel, M. Eschrig, T. Wagner, S. Komori, A. Srivastava, J. W. A. Robinson *et al.*, Effect of Meissner screening and trapped magnetic flux on magnetization dynamics in thick Nb/Ni<sub>80</sub>Fe<sub>20</sub>/Nb trilayers, *Phys. Rev. Appl.* **11**, 014061 (2019).
- [52] C. Kittel, On the theory of ferromagnetic resonance absorption, *Phys. Rev.* **73**, 155 (1948).
- [53] D. Monroe, M. Alidoust, and I. Žutić, Tunable planar Josephson junctions driven by time-dependent spin-orbit coupling, *Phys. Rev. Appl.* **18**, L031001 (2022).